Multimode Optimization of Switched Reluctance Machines in Hybrid Electric Vehicles

Kaikai Diao, *Student Member, IEEE*, Xiaodong Sun, *Senior Member, IEEE*,
Gang Lei, *Member, IEEE*, Youguang Guo, *Senior Member, IEEE*,
and Jianguo Zhu, *Senior Member, IEEE*

***Abstract*- The belt-driven starter/generator (BSG), as a cost-effective solution, has been widely employed in hybrid electric vehicles (HEVs) to improve the stability and reduce the fuel consumption of the vehicles. It can provide more than 10% reduction in CO_2. Electrical machine is the heart of the BSG system, which is functioned both as motor and generator. In order to optimize both aspects of motor and generator simultaneously, this paper presents a new multimode optimization method for the switched reluctance machines. First, the general multimode concept and optimization method are presented. The switched reluctance motor and the switched reluctance generator are the two operation modes. The optimization models are established based on motor and generator functions. Sensitivity analysis, surrogate models and genetic algorithms are employed to improve the efficiency of the multimode optimization. Then, a design example of a segmented-rotor switched reluctance machine (SSRM) is investigated. Seven design variables and four driving modes are considered in the multiobjective optimization model. The Kriging model is employed to approximate the finite element model (FEM) in the optimization. Finally, the optimization results are depicted, and an optimal solution is selected. The comparison between the initial and optimal designs shows that the proposed method can improve the foremost performance of the SSRM under all driving modes.**

***Index Terms*- Belt-driven starter/generator (BSG), hybrid electric vehicles (HEVs), multimode optimization, switched reluctance motor (SRM).**

Manuscript received July 11, 2020; revised September 16, 2020 and December 03, 2020; accepted December 20, 2020. This work was supported in part by the National Natural Science Foundation of China under Project 51875261, in part by the Natural Science Foundation of Jiangsu Province of China under Project BK20180046, in part by the "Qinglan project" of Jiangsu Province, in part by the Postgraduate Research & Practice Innovation Program of Jiangsu Province under Project KYCX20_3014, and in part by the State Scholarship Fund of China Scholarship Council under Grant 202008320572. (*Corresponding author: Xiaodong Sun.*)

K. Diao and X. Sun are with the Automotive Engineering Research Institute, Jiangsu University, Zhenjiang 212013, China (email: diaokaikai@163.com, xdsun@ujs.edu.cn).

G. Lei and Y. Guo are with the School of Electrical and Data Engineering, University of Technology Sydney, NSW 2007, Australia (e-mail: Gang.Lei@uts.edu.au, Youguang.Guo-1@uts.edu.au).

J. Zhu is with the School of Electrical and Information Engineering, University of Sydney, NSW, 2006, Australia (e-mail: jianguo.zhu@sydney.edu.au).

I. Introduction

The simple structure, low cost, and the absence of permanent magnets make the switched reluctance machine a suitable candidate for the advanced flexible drivetrain [1], [2]. Due to its high robustness, a switched reluctance machine can be designed as a motor in most applications and functioned as a generator in harsh environments [3], [4]. For example, the belt-driven starter/generator (BSG) in which the core is the electric machine, is widely employed in hybrid electric vehicles (HEVs) to improve the stability and reduce fuel consumption. The machine in the BSG system is functioned both as motor and generator [5].

The switched reluctance motor (SRM) and the switched reluctance generator (SRG) are the two operation modes of the switched reluctance machine [6], [7]. In the motor mode, the phase is excited when the inductance is on the rise, while in generator mode, the phase is excited when the inductance decreases [8]. To improve power density, efficiency, and reduce the torque ripple, optimization is a necessary step in the design process of switched reluctance machines [9]. Previous optimization methods can be classified into two aspects, the single-objective optimization and the multiobjective optimization [10], [11]. For the single-objective optimization, it addresses only one performance. The problem with this single-objective optimization is that the potential influence on other important indices [12], [13]. Therefore, the multiobjective optimization as the trade-offs to the overall performance is preferred and becoming essential to the application-oriented design in switched reluctance machines [14]. Some popular design requirements, such as torque, efficiency, torque ripple, and cost, can be considered at the same time [15], [16].

With the fast development of numerical analysis method, optimization problems of switched reluctance machines can be efficiently solved by means of finite element analysis (FEA) with surrogate models and intelligent algorithms [17], [18]. Surrogate models such as response surface model (RSM) [19] and Kriging model [20] have been employed in multiobjective optimization problems to ease the computational burden. A set of optimization algorithms have been employed to find the optimal solution for the optimization, such as genetic algorithm (GA), differential evolution algorithm (DEA), particle swarm optimization (PSO) [21], [22].

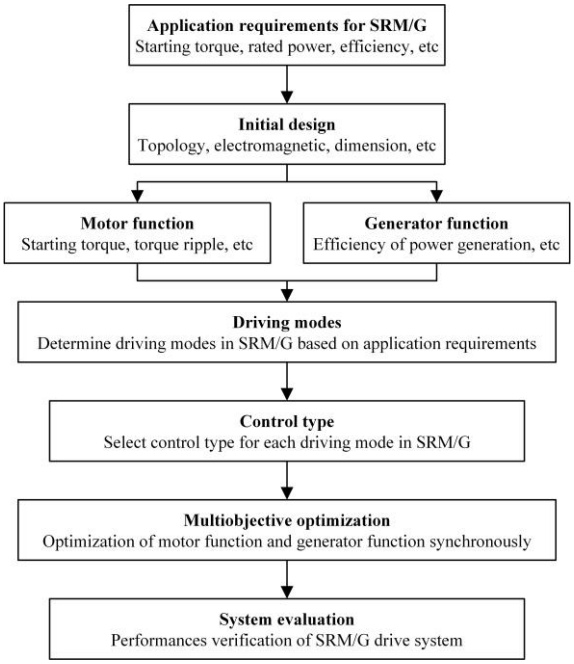

Fig. 1. Multimode design optimization framework for SRM/G.

A novel multiobjective system level optimization method for SRMs was proposed in our previous work [23], in which the parameters of the system including the motor level and control level are optimized simultaneously. On the other hand, for the SRG application, in [13], an SRG was designed for a variable wind energy conversion system. The firing angles and DC-link voltage are two objectives optimized for each rotor speed. It was found that the proposed approach returns a good compromise between high efficiency and low torque ripple.

The optimization methods mentioned above only put emphasis on one operating condition of the electrical machine, and the rated operation condition is mostly used. However, the motors and the generators mostly operate on different conditions, especially in the application of HEVs. There exist multiple driving cycles in HEVs, such as starting, normal cruise, climbing, acceleration and deceleration, and the key parameters in each driving cycle may have different importance [24]. Various driving cycles require more than one driving mode of the motor/generator. Thus, it is necessary to find a multimode optimization method with the combination of requirements under different driving modes. Previous multimode optimization methods are mainly conducted under motor mode. For switched reluctance machines, few papers investigate the optimization under the consideration of different driving modes as motor and generator. In HEVs, the electric machine is coupled with an internal combustion engine (ICE), and the regenerative model can absorb most of the released energy during braking. The switched reluctance machine is ideal for HEVs due to its excellent mechanical and thermal robustness [25]-[27]. The overall optimization of the switched reluctance machine functioned as switched reluctance motor/generator (SRM/G) considering multimode operation puts forward higher design requirements. Furthermore, the key points considered in the motor and generator are not the same. To meet the challenging requirements under the operation modes both in motor and generator aspects, it is meaningful to improve the capability of multimode operation of SRM/G systems. Besides, the design variables should be determined considering all the related driving modes both under motor and generator functions.

This paper presents a new multimode optimization method for switched reluctance machines considering driving modes both in motor and generator aspects. The corresponding control method is determined for each driving mode. Both the motor and generator functions are optimized by the multiobjective optimization method. The optimization objectives are selected from each driving mode to form the multiobjective optimization model. The main contributions of this paper can be summarized as follows.

(1) A comprehensive multimode optimization strategy considering the aspects of motor and generator is proposed, which is required for the application where mechanical energy and electrical energy convert to each other.

(2) In order to improve the quality of energy conversion comprehensively, a multiobjective method is presented in which the objectives of driving modes in motor and generator functions are selected as the optimization objectives.

(3) A segmented-rotor switched reluctance machine (SSRM) is selected as the optimization example, which is applied for the BSG. Four driving modes under motor/generator are investigated and optimization objectives selected of each mode are integrated into the multiobjective optimization.

The remainder of this paper is organized as follows. Section II presents the multimode concept and the optimization method. To verify the practicability and effectiveness of the proposed method, an example study for the optimization of an SSRM for HEV application is investigated in Section III. Specific implementation and results are provided in Section IV, followed by the conclusions in Section V.

II. Multimode Concept and Optimization Method

As mentioned above, the switched reluctance machine can be functioned as a motor and a generator. Fig. 1 shows a brief framework for the multimode design optimization of SRM/G. This kind of method has taken into consideration the motor function and generator function simultaneously. It can be divided into the following seven steps.

Step 1: Determine the application requirements for the SRM/G drive system.

The requirements for the SRM/G drive system conclude operation demands for the motor and the generator. On the motor aspect, torque and torque ripple mostly are the prime performances, while the efficiency of power generation is the foremost performance on the generator aspect.

Step 2: Initial design of the SRM/G.

This is a fundamental step, and it will affect the following optimization step. The initial specifications of the SRM/G can be derived according to the design theory and experience.

Step 3: Divide the optimization into motor function and generator function.

The key point in this optimization method is the consideration of the motor function and generator function simultaneously. Requirements in motor function and generator function are not the same in most applications [8], [18]. Previous works mostly concentrate on one function rather than the two functions. Theoretically, the cooperation of the motor and generator into the optimization process simultaneously is more suitable for some applications which utilize the functions of motor and generator.

Step 4: Determine driving modes in SRM/G.

In the actual application, many demands will be presented for the SRM/G. It is meaningful to divide the numerous driving modes of the SRM/G to achieve fundamental demands.

Step 5: Select the suitable control type for each mode.

A variety of control methods have been proposed for the SRMs, such as conventional current chopping control (CCC), angle position control (APC), direct torque control (DTC), and model predictive control (MPC). They provide alternatives for the control type of SRM/G.

Step 6: Perform the multiobjective optimization.

The multiobjective optimization models considering each driving mode under motor function and generator function can be established as follows.

$$\min: \begin{cases} f_{mi}(\mathbf{x}),\ i=1,2,\ldots,M \\ f_{gj}(\mathbf{x}),\ j=1,2,\ldots,G \end{cases} \tag{1}$$

where $f_{mi}(\mathbf{x})$ and $f_{gj}(\mathbf{x})$ are the functions of driving modes in motor function and generator function, respectively, and M and G are the numbers of optimization objectives in motor function and generator function, respectively.

Step 7: System evaluation.

The performances of driving modes in motor function and generator function are evaluated in this step.

As each driving mode in SRM/G has their own essential performance indices, there will exist a set of optimization objectives. The design variables should be optimized combined with their related driving modes. The detailed optimization flowchart is described in Fig. 2, which contains the following steps.

Step 1: Initial design of switched reluctance machine drive system.

The application requirements are achieved first, and the switched reluctance machine is initially designed according to the design theory base on the requirements. Normally, only the rated operation mode is taken into consideration in the design process, and the other performances are verified by FEA after the design. Then, the driving modes of the motor function and generator function are divided according to the operation modes in terms of the specific application. Finally, the control methods applied to each driving mode need to be determined.

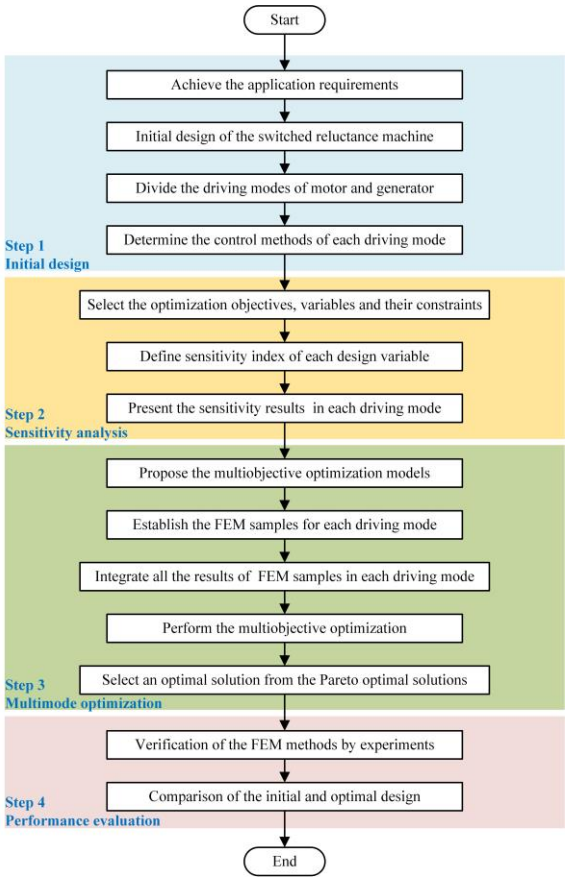

Fig. 2. Flowchart of the multimode optimization method.

Step 2: Sensitivity analysis of each variable.

Since this is a multimode optimization problem, the foremost requirement in each mode may not be the same. Sensitivity analysis is utilized to distinguish the importance of variables under each driving mode. The step will contribute to simplify the optimization process and ease the computational burden. The significant design variables which have a great influence on the optimization objectives will be selected for each driving mode according to the sensitivity results. The non-significant variables keep the initial values in the optimization process.

Step 3: Multimode optimization.

First, according to the optimization objectives in each driving mode, the multiobjective optimization models considering each driving mode under motor function and generator function are established. Second, the FEM models for each driving mode are established. Then, the results of FEM samples in each driving mode are integrated for the optimization program. Finally, the multiobjective optimization is conducted and an optimal solution can be selected from the Pareto optimal solutions.

Step 4: Performance evaluation.

In this step, the results obtained from FEM should be verified first, and then it will be convincing to compare the results between the initial design and the optimal solution.

III. A Design Example

In this example, an SSRM is designed for BSG application in HEVs. Fig. 3 illustrates the structure of the BSG system. The M/G in the figure functioned as the motor and generator is connected to ICE by the belt. The M/G can supply the extra power for the ICE when the vehicle starts, climbs or accelerates. Besides, it can convert mechanical energy into electricity and charge the batteries.

An SSRM topology was proposed in the previous work which inherits the innate benefits of switched reluctance machines, such as high fault tolerance and simple structure. Besides, it exhibits lower torque ripple and higher torque density [28]. Figs. 4 and 5 show the configuration and topology of the SSRM, respectively. As shown, the stator of this SSRM is composed of excited and auxiliary poles. The excited poles are wound by windings, while the auxiliary poles are only functioned as flux return paths without any windings. The rotor contains a series of discrete segmented rotors, and each component is embedded in the nonmagnetic isolator. The requirements of the SSRM for the BSG application are shown in Table I.

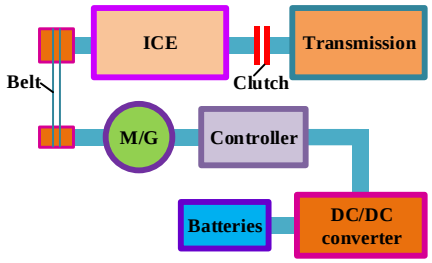

Fig. 3. BSG system

.

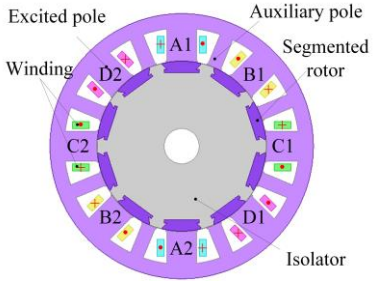

Fig. 4. Configuration of the SSRM.

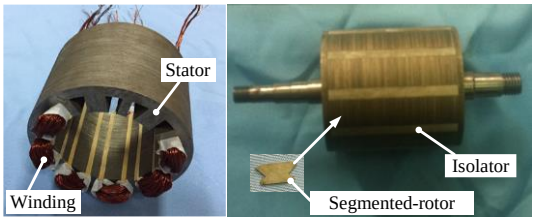

Fig. 5. The topology of the SSRM.

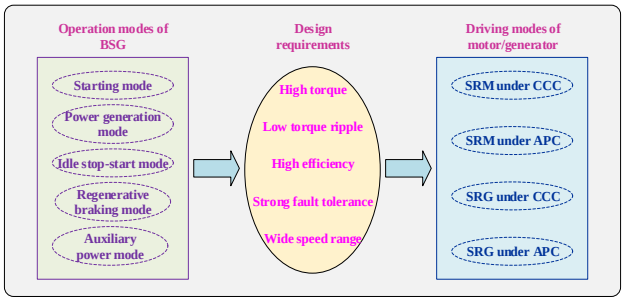

Fig. 6. Relationships among operation modes of BSG, design requirements and driving modes of SRM/G.

TABLE I
Specifications of the BSG Machine

Parameters	Unit	value
Rated power	kW	1.8
Rated speed	r/min	6000
Rated voltage	V	60
Transmission ratio of belt pulley	-	2.7:1
Startup torque	Nm	>24
Efficiency at rated speed	-	0.85

A. Operation modes of BSG

Fig. 6 shows the relationship between the operation modes of BSG, design requirements and driving modes of SRM/G. Generally, there are five main operation modes for the BSG system, i.e., starting mode, power generation mode, idle stop-start mode, regenerative braking mode and auxiliary power mode. Detailed expressions about each mode are illustrated as follows.

1) Starting mode: In this mode, the BSG machine is functioned as a starter, and it drags the ICE to the initial operation speed. The time is noticeably short and large torque is required in this progress.

2) Power generation mode: In this mode, the BSG machine converts the mechanical energy of the ICE into electricity and charges the batteries.

3) Idle stop-start mode: Beneficial from this mode in HEVs, about 10~15% fuel can be saved on the urban road when it is compared to the traditional vehicles. Furthermore, the emissions can be greatly reduced under this operation mode, especially when the car is waiting for the traffic light or in traffic jams.

4) Regenerative braking mode: The vehicle will generate the braking torque when the throttle is released, or the brake is pressed. The BSG can absorb the kinetic energy and convert it into electricity.

5) Auxiliary power mode: In this mode, the BSG provides extra electrical power to add the output power. It always operates at the quick start, climbing and acceleration driving cycles.

B. Driving modes

According to the requirements of the five main operation modes, the SRM/G needs to operate under the different

driving modes during the whole operation region in both motor function and generator function. Based on the mature control methods of SRM/G, such as current chopping control (CCC) and angle position control (APC), the driving modes can be divided as follows.

1) SRM under CCC method (SRM-CCC): It means the SRM/G is operated as a motor, and the corresponding control method is the CCC method. This mode is used during the starting mode at the low speed. In this driving mode, the output torque is the foremost requirement, thus it is selected as the single optimization objective at SRM-CCC mode.

2) *SRM under APC method (SRM-APC)*: In this driving mode, the SRM operates under the APC method. Since the motor mostly runs under the high speed, it can provide extra power for the vehicle and save the fuel. To improve the ride comfort and operation reliability in this driving mode, the torque ripple is selected to be the optimization objective.

3) *SRG under CCC method (SRG-CCC)*: In the regenerative braking operation mode, the CCC method is utilized to realize the energy conversion under the low speed of the SRG. The efficiency of power generation usually needs to be paid more attention in SRG-CCC driving mode.

4) *SRG under APC method (SRG-APC)*: When the vehicle is in normal operation, the SRG charges the batteries under the APC method. It mostly works under the power generation mode of BSG. High efficiency is the primary goal in this mode.

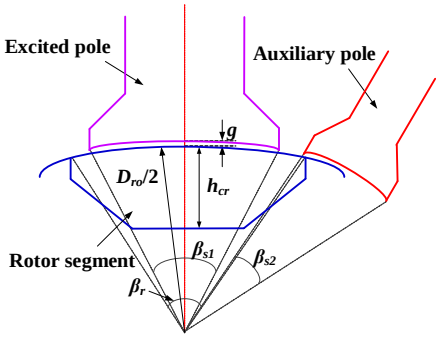

Fig. 7. Parametric model of the SSRM.

TABLE II
DESIGN VARIABLES OF THE SSRM

Par.	Description	Variation range
D_{ro}	Rotor outer diameter	[75 mm, 85 mm]
β_{s1}	Excited stator pole arc	[19°, 21.5°]
β_{s2}	Auxiliary stator pole arc	[9°, 11°]
β_r	Rotor pole arc	[24°, 30°]
L_{sy}	Stator yoke length	[5 mm, 9 mm]
h_{cr}	Height of segmented rotor	[4 mm, 7 mm]
g	Air gap	[0.25 mm, 0.5 mm]

C. Optimization models and variables

According to the analysis above, to meet the requirements of each driving mode, the multiobjective model of the multimode optimization problem can be defined as

$$\min: \begin{cases} f_{m1}(\mathbf{x}) = -T_{m1\_avg} \\ f_{m2}(\mathbf{x}) = T_{m2\_ripple} \\ f_{g1}(\mathbf{x}) = -\eta_{g1} \\ f_{g2}(\mathbf{x}) = -\eta_{g2} \end{cases} \tag{2}$$

where f_{m1} and f_{m2} are the functions of SRM-CCC and SRM-APC driving modes, respectively, f_{g1} and f_{g2} are the functions of SRG-CCC and SRG-APC driving modes, respectively, T_{m1_avg} is the average output torque, T_{m2_ripple} is the torque ripple, and η_{g1} and η_{g2} are the power generation efficiencies of SRG-CCC and SRG-APC driving modes, respectively. The parametric model of the SSRM is shown in Fig. 7, and the design variables and their corresponding variation ranges are listed in Table II.

The torque ripple is defined as

$$T_{rippple} = \frac{T_{\max} - T_{\min}}{T_{avg}} \tag{3}$$

where T_{max}, T_{min}, and T_{avg} are the maximum, minimum, and average torques, respectively [29].

The efficiency of power generation can be calculated by

$$\eta = \frac{T_{avg} \cdot \omega - P_{loss}}{T_{avg} \cdot \omega} \tag{4}$$

where ω is the angle speed, and P_{loss} is the average loss which contains copper loss and core loss.

IV. IMPLEMENTATION AND RESULTS

The discussion of the optimization method is based on the results of the finite element model (FEM). Thus, the first step is to verify the reliability of the data achieved from FEM. Second, local sensitivity analysis is carried out to select the significant optimization parameters. Third, the proposed multiobjective optimization process considering driving modes in SRM/G is performed. Then, the results achieved from the Kriging model are verified by the FEM results. Finally, the comparison between the selected optimal solution and the initial design is investigated, and the results are further presented and discussed.

A. Verification of FEM

Fig. 8 shows the platform for the SSRM drive system. The simulation model is established in Ansoft/Maxwell, and the control methods of CCC and APC are implemented in the external circuit connected to the model. The comparisons of flux linkage and instantaneous torque between simulation and measured results are shown in Figs. 9 and 10, respectively. It is found that the estimated performance parameters achieved from the FEM are well aligned with the experiment results. Besides, the iron loss in FEM under the rated operation is 126.9 W while that achieved by experiment is 134.89 W. the error of iron loss between is about 6.3%, and it can be explained by the influence of mesh operations in FEM and the assembly process. All the measured results can verify the effectiveness of the simulation results, and further prove the

reliability of the FEM. Thus, the FEM samples prepared for the optimization are reliable. More details, including HIL platform verification, can be found in [25].

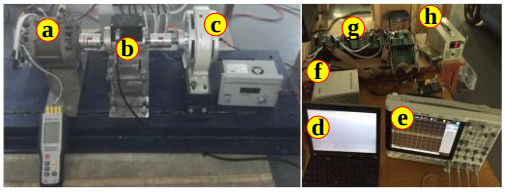

Fig. 8. The platform of the investigated SSRM drive system. (a) The 16/10 SSRM. (b) Torque and speed sensor. (c) Magnetic powder brake. (d) PC. (e) Oscilloscope. (f) dSPACE. (g) Power converter and driving circuit. (h) Power supply.

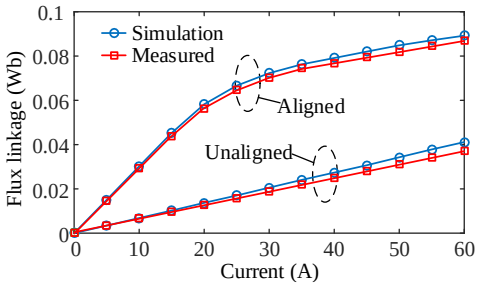

Fig. 9. Simulation and measured results of flux linkage.

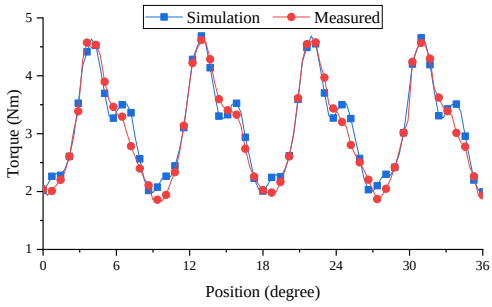

Fig. 10. Instantaneous torque comparison between simulation and experiment.

B. Sensitivity analysis

To select the significant variables in each driving mode, the local sensitivity analysis, which can reflect the influence/sensitivity of each parameter on the performances, are performed [30]. Mathematically, the sensitivity of the *i*th parameter x_i at the point $\mathbf{x_0}$ can be defined as

$$S_i = \left.\frac{\partial f(\mathbf{x})}{\partial x_i}\right|_{\mathbf{x}=\mathbf{x}_0} \tag{5}$$

where S_i is the sensitivity, and $f(\mathbf{x})$ is the objective function. In this paper, $f(\mathbf{x})$ refers to average torque in SRM-CCC, torque ripple in SRM-APC, and efficiencies of power generation in SRG-CCC and SRG-APC, respectively.

The sensitivity analysis is based on the FEA, and there is no accurate analytical expression for the objective functions of this SSRM. In this case, a differential form is taken to calculate S_i. It should be noted that the sensitivities of different parameters calculated by (5) have different units, thus a normalization step considering absolute value is carried out as

$$SA_i = \left|\frac{\left[f(\mathbf{x}_0 \pm \Delta\mathbf{x}_i) - f(\mathbf{x}_0)\right] / f(\mathbf{x}_0)}{\pm\Delta x_i / x_i}\right| \tag{6}$$

The detailed analysis steps are presented as follows. First, we apply ±20% perturbations to each variable x_i, and based on (6), calculate the objective function corresponding to the two samples, i.e., (1-20%)x_i and (1+20%)x_i. Second, calculate the relative errors of these two samples by comparing the objective function of these two samples to that obtained from the initial example. Finally, the average of absolute values of these two relative errors is taken as the sensitivity value. As there are seven variables in this example, for each driving mode, it requires 15 samples including 14 (2x7) samples for these perturbations and one initial sample. Totally, it requires 60 samples in the four driving modes in this example.

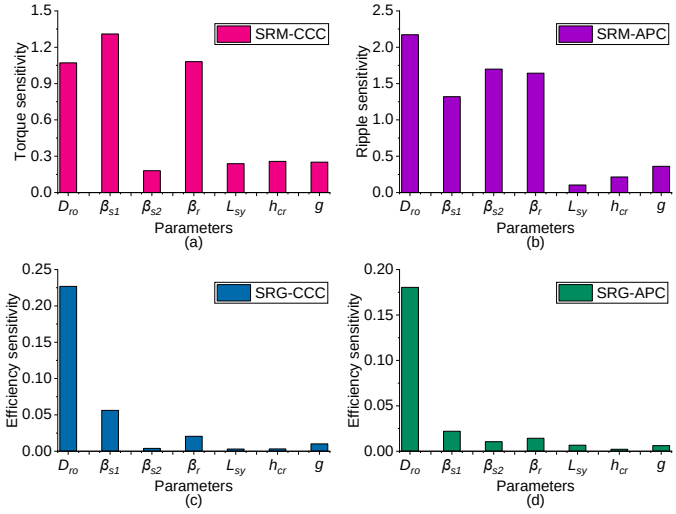

Fig. 11. Sensitivity analysis results of each variable in each driving mode. (a) SRM-CCC. (b) SRM-APC. (c) SRG-CCC. (d) SRG-APC.

TABLE III
SELECTION OF SENSITIVE VARIABLES

Driving modes	Sensitive variables	Representative speed
SRM-CCC	D_{ro}, β_{s1}, β_r	$n = 0.1n_{\text{rated}}$
SRM-APC	D_{ro}, β_{s1}, β_{s2}, β_r	$n = n_{\text{rated}}$
SRG-CCC	D_{ro}	$n = 0.1n_{\text{rated}}$
SRG-APC	D_{ro}	$n = n_{\text{rated}}$

Fig. 11 shows the local sensitivity analysis results of each design variables in each driving mode. In the SRM-CCC mode, the optimization objective is the average torque, and D_{ro}, β_{s1}, and β_r are selected as the optimization parameters, as shown in Fig. 11(a). In the SRM-APC mode, four design variables, i.e., D_{ro}, β_{s1}, β_{s2}, and β_r are selected as the optimization parameters according to the torque ripple sensitivity results, as shown in Fig. 11(b). Moreover, D_{ro} is the only significant parameter in

SRG-CCC mode and SRG-APC mode, as shown in Figs. 11(c) and (d). The sensitive variables and representative speeds of each driving mode are tabulated in Table III.

C. Multimode optimization

After determination of the significant parameters in each driving mode, the specific optimization models of the proposed example related to the optimization parameters can be defined as

$$\min: \begin{cases} f_{m1}(D_{ro},\ \beta_{s1},\ \beta_r) = -T_{m1\_avg} \\ f_{m2}(D_{ro},\ \beta_{s1},\ \beta_{s2},\ \beta r) = T_{m2\_ripple} \\ f_{g1}(D_{ro}) = -\eta_{g1} \\ f_{g2}(D_{ro}) = -\eta_{g2} \end{cases}. \tag{7}$$

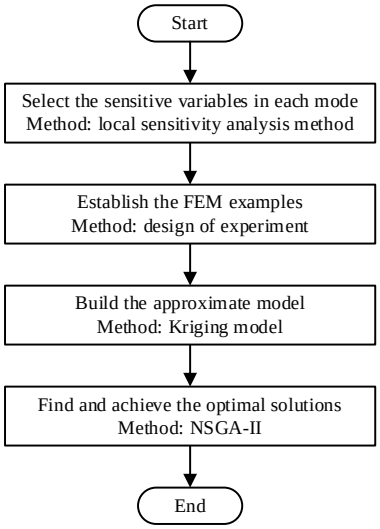

Fig. 12. Optimization process.

As shown, each driving mode has its own optimization objective and optimization variables. The total optimization framework of this investigated example is shown in Fig. 12.

For the SRM-CCC driving mode, it requires 252 (6x6x7, where 6, 6 and 7 are the sampling numbers of variables D_{ro}, β_{s1}, and β_r) FEM samples. For the SRM-APC driving mode, it requires 1260 (6x6x5x7, where 6, 6, 5, and 7 are the sampling numbers of variables D_{ro}, β_{s1}, β_{s2}, and β_r) FEM samples. Besides, only 6 (where 6 is the sampling number of variable D_{ro}) FEM samples are required in SRG-CCC and SRG-APC driving modes, respectively. To avoid the mutual influences between the optimization variables, it is better optimizing all the variables in one function. Thus, all the FEM samples of the four driving modes are integrated and then sent to perform the Kriging model.

Kriging model is superior in the modeling of local nonlinearities since it includes both mean trend and variances of the responses compared with others, such as response surface model (RSM) and radial basis functions (RBF) [14, 22]. Given n sample points $\{x_1, x_2, ..., x_n\}$ and their responses $\{y(x_1), y(x_2), \ldots, y(x_n)\}$, for an input $\mathbf{x}$, the response $y(\mathbf{x})$ of the Kriging model can be expressed as

$$\hat{y}(\mathbf{x}) = F(\boldsymbol{\beta}, \mathbf{x}) + z(\mathbf{x}) \tag{8}$$

where $F(\boldsymbol{\beta},\mathbf{x})$ is the regression model and $z(\mathbf{x})$ is a random error term used for the modeling of local deviation. $F(\boldsymbol{\beta},\mathbf{x})$ is represented as

$$F(\boldsymbol{\beta}, \mathbf{x}) = \beta_1 f_1(\mathrm{x}) + \cdots + \beta_p f_p(\mathrm{x}) = f(\mathbf{x})^T \boldsymbol{\beta} \tag{9}$$

The coefficients β_k are regression parameters and $f(x)$ is a known approximation model. $z(\mathbf{x})$ is usually assumed to be a vector with mean of zero, covariance σ^2.

In the optimization program, there are four optimization variables, i.e., D_{ro}, β_{s1}, β_{s2}, and β_r, and four optimization objectives, i.e., T_{m1_avg} in SRM-CCC mode, T_{m2_ripple} in SRM-APC mode, η_{g1} in SRG-CCC mode, and η_{g2} in SRG-APC mode. As β_{s2} is the non-significant parameter in the SRM-CCC mode, thus in the list of samples after integration, different values of β_{s2} with the same values of the significant parameters will have the same results on T_{m1_avg}. Same methods are utilized in the SRG-CCC and SRG-APC modes when integrating the FEM samples.

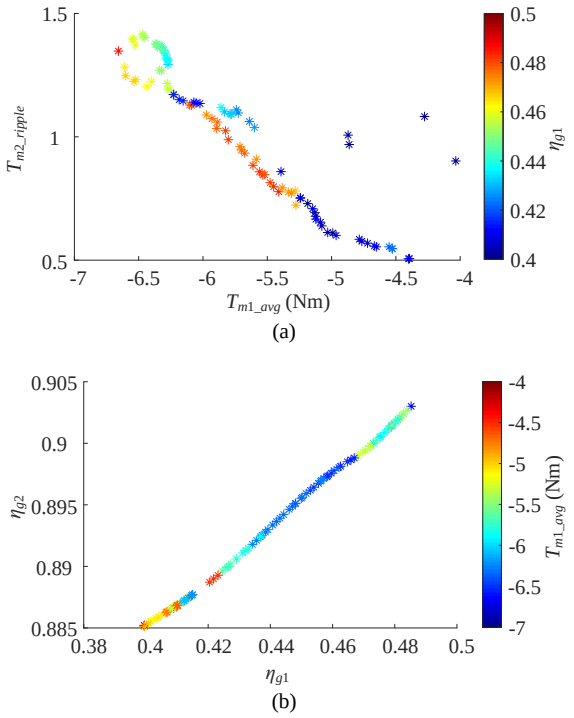

Fig. 13. Pareto optimal solutions. (a) View of T_{m1_avg}, T_{m2_ripple}, and η_{g1}. (b) View of T_{m1_avg}, T_{m2_ripple}, and η_{g2}.

Fig. 13 depicts the Pareto optimal solutions. Fig. 13(a) illustrates the relationship between T_{m1_avg}, T_{m2_ripple} and η_{g1}, and Fig. 13(b) illustrates the relationship between η_{g1}, η_{g2}, and T_{m1_avg}. From Fig. 13, several conclusions can be drawn.

1) The average torque in SRM-CCC mode is contradictory to the torque ripple in SRM-APC mode. Which means achieving high torque in SRM-CCC will sacrifice torque ripple performance in SRM-APC. The prime performances in

different driving modes are corrected with the change of design variables.

2) The high efficiency of power generation is concentrated in the middle torque region, as shown in Fig. 13(a). Thus, in this area, a better balance between T_{m1_avg}, T_{m2_ripple}, η_{g1} and η_{g2} can be achieved, i.e., middle values of T_{m1_avg} and T_{m2_ripple}, and high values of η_{g1} and η_{g2}.

3) It can be found in Fig. 13(b), although the control methods in SRG-CCC and SRG-APC modes are different, η_{g1} is proportional to η_{g2}. However, the efficiency range of η_{g1} is only 40~50% in the low speed under CCC, while the efficiency of η_{g2} is higher than 88% in the high speed under APC.

D. Verification of Kriging model

Approximate models act as an alternative for FEA and MEC models, which ease the computational burden. In the optimization process, the Kriging model is utilized to approximate the model based on the simulation data of the FEM samples. To ensure the accuracy of the multiobjective optimization, it is necessary to verify the effectiveness of the Kriging model. The quick way is to compare the results from the approximate model with those from FEM. In this paper, all the samples are included in this example, the root mean square error of f_{m1}, f_{m2}, f_{g1}, and f_{g2} are 0.1776 Nm, 0.0512 Nm, 0.24% and 0.06%, respectively, which are corresponding to 0.71%, 0.06%, 0.51% and 0.07% of initial values, respectively. Thus, the errors of the Kriging model are acceptable.

TABLE IV
SSRM PARAMETERS AND PERFORMANCE OF THE INITIAL AND OPTIMAL DESIGNS

Par.	Unit	Initial	Optimal
D_{ro}	mm	82.00	77.80
β_{s1}	deg.	21.38	20.04
β_{s2}	deg.	10.69	9.40
β_r	deg.	26.64	27.19
L_{sy}	mm	7.00	7.00
h_{cr}	mm	5.50	5.50
g	mm	0.25	0.25
N	-	24	24
T_{m1_avg}	Nm	25.15	27.05
T_{m2_ripple}	%	85.80	68.67
η_{g1}	%	46.94	48.40
η_{g2}	%	90.01	90.27

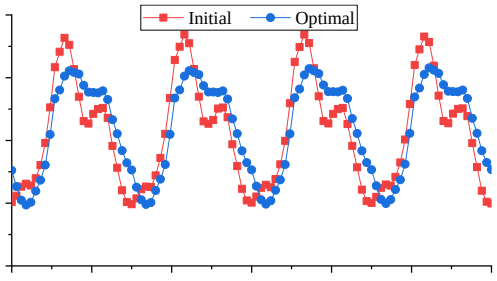

Fig. 14. Torque comparison between the initial design and the optimal solution in SRM-APC mode.

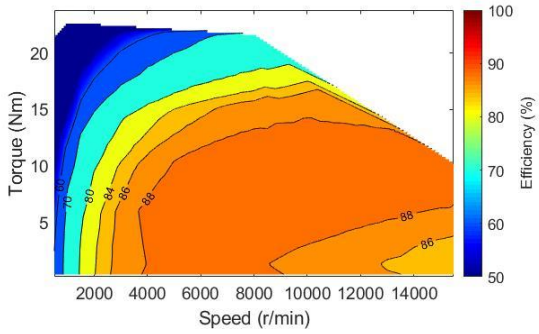

Fig. 15. Efficiency map of the optimal design.

E. Results comparison

In order to quantitatively illustrate the superiority of the optimization results, an optimal solution is selected to meet the requirements of high start torque, low torque ripple and high efficiency of power generation. Detailed comparison of the values between the initial design and the optimal solution is listed in Table IV. It can be seen that the selected optimal solution improves the performances of the foremost objective in all the driving modes. Fig. 14 illustrates the torque compassion between the initial and the optimal designs in SRM-APC mode. It can be found that the initial design and the optimal solution exhibit close average torque. However, the SSRM with the optimal solution exhibits smaller torque ripple than the SSRM with the initial design. Fig. 15 shows the efficiency map of the optimal solution functioned as the motor. The high-efficiency area of the optimal solution ranges approximately from 4000 to 14000 r/min. Besides, the efficiency at the rated running point is more than 85%, which satisfies the specification listed in Table I.

V. CONCLUSION

In this paper, a new comprehensive multiobjective optimization method considering different driving modes of SRM/G was presented. The presented method provided an efficient design and optimization solution for the electrical machine functioned as motor and generator in some specific applications like HEVs. An example of an SSRM applied in BSG system was investigated to verify the feasibility of the proposed method. In the implementation, four driving modes, i.e., SRM-CCC, SRM-APC, SRG-CCC, and SRG-APC, in SRM/G were determined according to the operation modes of BSG. The significant design variables were selected for each driving mode by the sensitivity analysis, and the results of FEM samples in each driving mode were integrated for the optimization. An optimal solution was selected for the requirements of high starting torque, low torque ripple and high efficiency of power generation. The comparison between the initial and the selected solution shows that the proposed

method can provide an optimal solution to meet the requirements of different driving modes in SRM/G.

REFERENCES

[1]. S. Li, S. Zhang, J. Dang, T. G. Habetler, and R. G. Harley, "Analytical calculation of the phase inductance profile of switched reluctance machines," *IEEE Trans. Energy Convers.*, vol. 34, no. 3, pp. 1149-1163, 2019.

[2]. X. Sun, L. Feng, K. Diao, and Z. Yang, "An improved direct instantaneous torque control based on adaptive terminal sliding mode for a segmented-rotor SRM," *IEEE Trans. Ind. Electron.*, 2020, to be published.

[3]. F. Peng, J. Ye, and A. Emadi, "A digital PWM current controller for switched reluctance motor drives," *IEEE Trans. Power Electron.*, vol. 31, no. 10, pp. 7087-7098, 2016.

[4]. L. Qiu, Y. Shi, J. Pan, B. Zhang, and G. Xu, "Positioning-tracking controller design of a linear motion control system based on vectorization technique," *IEEE/ASME Trans. Mechatron.*, vol. 23, no. 4, pp. 1512-1520, 2018.

[5]. X. Sun, Y. Shen, S. Wang, G. Lei, Z. Yang, and S. Han, "Core losses analysis of a novel 16/10 segmented rotor switched reluctance BSG motor for HEVs using nonlinear lumped parameter equivalent circuit model," *IEEE/ASME Trans. Mechatron.*, vol. 23, no. 2, pp. 747-757, 2018.

[6]. S. Li, S. Zhang, T. G. Habetler, and R. G. Harley, "Modeling, design optimization, and applications of switched reluctance machines—a review," *IEEE Trans. Ind. Appl.*, vol. 55, no. 3, pp. 2660-2681, 2019.

[7]. W. Ding and D. Liang, "A fast analytical model for an integrated switched reluctance starter/generator," *IEEE Trans. Energy Convers.*, vol. 25, no. 4, pp. 948-956, 2010.

[8]. J. Oh and B. Kwon, "Design, optimization, and prototyping of a transverse flux-type-switched reluctance generator with an integrated rotor," *IEEE Trans. Energy Convers.*, vol. 31, no. 4, pp. 1521-1529, 2016.

[9]. D. Gerada, X. Huang, C. Zhang, H. Zhang, X. Zhang, and C. Gerada, "Electrical machines for automotive electrically assisted turbocharging," *IEEE/ASME Trans. Mechatron.*, vol. 23, no. 5, pp. 2054-2065, 2018.

[10]. Z. Shi, X. Sun, Y. Cai, and Z. Yang, "Robust design optimization of a five-phase PM hub motor for fault-tolerant operation based on Taguchi method," *IEEE Trans. Energy Convers.*, vol. 35, no. 4, pp. 2036-2044. Dec. 2020.

[11]. K. Diao, *et al*, "System-level robust design optimization of a switched reluctance motor drive system considering multiple driving cycles," *IEEE Trans. Energy Convers.*, 2020, to be published.

[12]. X. Sun, Z. Shi, Y. Cai, G. Lei, Y. Guo, and J. Zhu, "Driving-cycle oriented design optimization of a permanent magnet hub motor drive system for a four-wheel-drive electric vehicle," *IEEE Trans. Transport. Electrific.*, vol. 6, no. 3, pp. 1115-1125, Sep. 2020.

[13]. P. J. d. S. Neto, T. A. d. S. Barros, M. V. d. Paula, R. R. d. Souza, and E. R. Filho, "Design of computational experiment for performance optimization of a switched reluctance generator in wind systems," *IEEE Trans. Energy Convers.*, vol. 33, no. 1, pp. 406-419, 2018.

[14]. X. Sun, Z. Shi, G. Lei, Y. Guo, and J. Zhu, "Multi-objective design optimization of an IPMSM based on multilevel strategy," *IEEE Trans. Ind. Electron.*, vol. 68, no. 1, pp. 139-148, Jan. 2021.

[15]. Z. Shi, *et al*, "Analysis and optimization of radial force of permanent magnet synchronous Hub motors," *IEEE Trans. Magn.*, vol. 56, no. 2, Feb. 2020, Art. no.: 7508804.

[16]. Z. Shi, X. Sun, Y. Cai, Z. Yang, G. Lei, Y. Guo, and J. Zhu, "Torque analysis and dynamic performance improvement of a PMSM for EVs by skew angle optimization," *IEEE Trans. Appl. Supercon.*, vol. 29, no. 2, pp. 1-5, 2019.

[17]. T. Raminosoa, B. Blunier, D. Fodorean, and A. Miraoui, "Design and optimization of a switched reluctance motor driving a compressor for a PEM fuel-cell system for automotive applications," *IEEE Trans. Ind. Electron.*, vol. 57, no. 9, pp. 2988-2997, 2010.

[18]. H. Chen, W. Yan, J. J. Gu, and M. Sun, "Multiobjective optimization design of a switched reluctance motor for low-speed electric vehicles with a Taguchi–CSO algorithm," *IEEE/ASME Trans. Mechatron.*, vol. 23, no. 4, pp. 1762-1774, 2018.

[19]. J. H. Lee, "Optimum shape design solution of flux switching motor using response surface methodology and new type winding," *IEEE Trans. Magn.*, vol. 48, no. 4, pp. 1637-1640, 2012.

[20]. S. I. Nabeta, I. E. Chabu, L. Lebensztajn, D. A. P. Correa, W. M. d. Silva, and K. Hameyer, "Mitigation of the torque ripple of a switched reluctance motor through a multiobjective optimization," *IEEE Trans. Magn.*, vol. 44, no. 6, pp. 1018-1021, 2008.

[21]. E. Öksüztepe, "In-wheel switched reluctance motor design for electric vehicles by using a Pareto-based multiobjective differential evolution algorithm," *IEEE Trans. Veh. Technol.*, vol. 66, no. 6, pp. 4706-4715, 2017.

[22]. B. Mirzaeian, M. Moallem, V. Tahani, and C. Lucas, "Multiobjective optimization method based on a genetic algorithm for switched reluctance motor design," *IEEE Trans. Magn.*, vol. 38, no. 3, pp. 1524-1527, 2002.

[23]. K. Diao, X. Sun, G. Lei, Y. Guo, and J. Zhu, "Multiobjective system level optimization method for switched reluctance motor drive systems using finite-element model," *IEEE Trans. Ind. Electron.*, vol. 67, no. 12, pp. 10055-10064, 2020.

[24]. X. Sun, Z. Shi, and J. Zhu, "Multi-objective design optimization of an IPMSM for EVs based on fuzzy method and sequential Taguchi method," *IEEE Trans. Ind. Electron.*, 2020, to be published.

[25]. X. Sun, K. Diao, G. Lei, Y. Guo, and J. Zhu, "Real-time HIL emulation for a segmented-rotor switched reluctance motor using a new magnetic equivalent circuit," *IEEE Trans. Power Electron.*, vol. 35, no. 4, pp. 3841-3849, 2020.

[26]. K. Kiyota, T. Kakishima, H. Sugimoto, and A. Chiba, "Comparison of the test result and 3D-FEM analysis at the knee point of a 60 kW SRM for a HEV," *IEEE Trans. Magn.*, vol. 49, no. 5, pp. 2291-2294, 2013.

[27]. A. Chiba, M. Takeno, N. Hoshi, M. Takemoto, S. Ogasawara, and M. A. Rahman, "Consideration of number of series turns in switched-reluctance traction motor competitive to HEV IPMSM," IEEE Trans. Ind. Appl., vol. 48, no. 6, pp. 2333-2340, 2012.

[28]. X. Sun, K. Diao, G. Lei, Y. Guo, and J. Zhu, "Study on segmented-rotor switched reluctance motors with different rotor pole numbers for BSG system of hybrid electric vehicles," *IEEE Trans. Veh. Technol.*, vol. 68, no. 6, pp. 5537-5547, 2019.

[29]. Z. Q. Zhu, B. Lee, L. Huang, and W. Chu, "Contribution of current harmonics to average torque and torque ripple in switched reluctance machines," *IEEE Trans. Magn.*, vol. 53, no. 3, pp. 1-9, 2017.

[30]. G. Lei, C. Liu, J. Zhu, and Y. Guo, "Techniques for multilevel design optimization of permanent magnet motors," *IEEE Trans. Energy Convers.*, vol. 30, no. 4, pp. 1574-1584, 2015.

Kaikai Diao (S'18) was born in Zhenjiang, Jiangsu, China, in 1994. He received the B.S. degree in vehicle engineering from Jiangsu University, Zhenjiang, China, in 2017, and he is currently working toward the Ph.D. degree in Jiangsu University, Zhenjiang, China.

His current research interests include design, optimization, magnetic equivalent circuits modeling, control, and loss analysis of switched reluctance motors for automobile application.

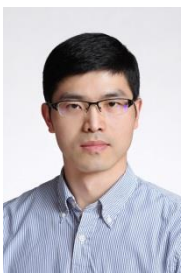

Xiaodong Sun (M'12-SM'18) received the B.Sc. degree in electrical engineering, and the M.Sc. and Ph.D. degrees in control engineering from Jiangsu University, Zhenjiang, China, in 2004, 2008, and 2011, respectively.

Since 2004, he has been with Jiangsu University, where he is currently a Professor in Vehicle

Engineering with the Automotive Engineering Research Institute. From 2014 to 2015, he was a Visiting Professor with the School of Electrical, Mechanical, and Mechatronic Systems, University of Technology Sydney, Sydney, Australia. His current teaching and research interests include electrical machines and drives, drives and control for electric vehicles, and intelligent control. He is the author or coauthor of more than 100 refereed technical papers and one book, and he is the holder of 42 patents in his areas of interest. Dr. Sun is an Editor of the IEEE TRANSACTIONS ON ENERGY CONVERSION.

Gang Lei (M'14) received the B.S. degree in Mathematics from Huanggang Normal University, China, in 2003, the M.S. degree in Mathematics and Ph.D. degree in Electrical Engineering from Huazhong University of Science and Technology, China, in 2006 and 2009, respectively.

He is currently a Senior Lecturer at the School of Electrical and Data Engineering, University of Technology Sydney (UTS), Australia. His research interests include computational electromagnetics, design optimization and control of electrical drive systems and renewable energy systems. He is an Associate Editor of the IEEE TRANSACTIONS ON INDUSTRIAL ELECTRONICS.

Youguang Guo (S'02-M'05-SM'06) received the B.E. degree from Huazhong University of Science and Technology, China in 1985, the M.E. degree from Zhejiang University, China in 1988, and the Ph.D. degree from University of Technology, Sydney (UTS), Australia in 2004, all in electrical engineering.

He is currently a Professor at the School of Electrical and Data Engineering, University of Technology Sydney (UTS). His research fields include measurement and modeling of properties of magnetic materials, numerical analysis of electromagnetic field, electrical machine design optimization, power electronic drives and control.

Jianguo Zhu (S'93–M'96–SM'03) received the B.E. degree in 1982 from Jiangsu Institute of Technology, Jiangsu, China, the M.E. degree in 1987 from Shanghai University of Technology, Shanghai, China, and the Ph.D. degree in 1995 from the University of Technology Sydney (UTS), Sydney, Australia, all in electrical engineering.

He was appointed a lecturer at UTS in 1994 and promoted to full professor in 2004 and Distinguished Professor of Electrical Engineering in 2017. At UTS, he has held various leadership positions, including the Head of School for School of Electrical, Mechanical and Mechatronic Systems and Director for Centre of Electrical Machines and Power Electronics. In 2018, he joined the University of Sydney, Australia, as a full professor and Head of School for School of Electrical and Information Engineering. His research interests include computational electromagnetics, measurement and modelling of magnetic properties of materials, electrical machines and drives, power electronics, renewable energy systems and smart micro grids.